Latin American Journal of Solids and Structures
www.lajss.org

Numerical Forensic Model for the Diagnosis of a Full-Scale RC Floor

Abstract

The paper presents the results of an investigation on the diagnosis and assessment of a full-scale reinforced concrete floor utilizing a 3-D forensic model developed in the framework of plasticity-damage approach. Despite the advancement in nonlinear finite element formulations and models, there is a need to verify models on nontrivial challenging structures. Various standards on strengthening existing structures consider numerical diagnosis as a major stage involving safety and economical aspects. Accordingly, model validity is a major issue that should preferably be examined against realistic large-scale tests. This was done in this study by investigating a one-story joist floor with wide shallow beams supported on columns. The surveyed cracking patterns on the entire top side of the floor were reproduced by the forensic model to a reasonable degree in terms of orientation and general location. Concrete principal plastic tensile strain was shown to be a good indirect indicator of cracking patterns. However, identifying the underlying reasons of major cracks in the floor required correlating with other key field parameters including deflections, and internal moments. Therefore, the ability of the forensic model to reproduce the surveyed damage state of the floor provided a positive indication on the material models, spatial representation, and parameter selection. Such models can be used as forensic tools for assessing the existing conditions as required by various standards and codes.

Keywords

nonlinear finite element; reinforced concrete; forensic; cracking; numerical model; diagnosis; existing structures.

Ahmed B. Shuraim*

Associate Professor, College of Engineering (Civil), King Saud University, Riyadh, Saudi Arabia

Received 30 Mar 2012;
In revised form 26 Apr 2012

* Author email: ashuraim@ksu.edu.sa

1 INTRODUCTION

Many existing Reinforced Concrete (RC) structures show a number of situations where the load carrying capacity of a structure in service may need to be increased, like where there is a change of loading of use, or where the structure has been damaged. With reference to

a deficient RC structure, three stages of assessment have been outlined by some structural design guidelines [1, 2] investigation of current conditions, diagnosis, selection of appropriate solution and strengthening design using FRP materials [11]. Because proper diagnosis has strong implications on various aspects of the structure including strength, strengthening cost, safety, etc., robust reliable 3-D forensic models are crucial for real life full- three dimensional structures.

Nonlinear finite element (NLFE) for reinforced concrete structures has many applications [4, 5] including: providing an insight into the behavior; predicting possible modes of failure; corroborating the experimental findings; and extending the findings to locations where measurements are not available. From the perspective of forensic studies in relation to damaged or ageing structures, NLFE can be can be of value to assess the safety and integrity of existing structures; identify causes of deficiencies; and to assess the behavior expected from retrofitted structures. However, NLFE models comprise various theories, elements and procedures where some limitations, shortcomings and complexity were reported [34, 35].

The complexity of finite element is in part due to the complexity of the concrete physical behavior, being largely determined by the properties and interaction among its constituent materials. To incorporate these experimentally-observed features into finite element, several constitutive modeling theories have been proposed, including: nonlinear elasticity, plasticity, and damage mechanics, among others [14, 18, 26]. Coupled damage-plasticity formulation can provide a better representation of salient concrete features [18, 26], which is among the concrete models incorporated in ABAQUS .

Numerical modeling of cracking in concrete usually involves either discrete or smeared cracking approaches [9, 16, 28]. Discrete approach represents a crack as a geometrical discontinuity and can be treated in the framework of fracture mechanics concepts. The main drawback is that one needs to know location of an expected crack and the direction along which it propagates [28]. On the contrary, smeared crack through damage mechanics offers the essential advantage of predicting the location of this critical flaw. To circumvent mesh-sensitivity and numerical divergence, an energy criterion can be employed instead of strength failure criterion. In ABAQUS, fictitious crack model introduced by Hillerborg (1985)[21] can be employed to alleviate the mesh-sensitivity. Whatever the chosen approach, numerical models need to be validated not only on the basis of small members with trivial geometry but rather on the basis of more challenging reinforced concrete structures [9].

This study developed a forensic model on the basis of ABAQUS formulations and numerous material models from the literature. The model capability was demonstrated over a full-scale building floor for the purpose of assessing its adequacy in predicting the overall behavior in terms of deformations and cracking patterns. Furthermore, the correlation between cracking and internal distribution of moments was established at critical sections, giving the background for the newly proposed design procedure [29, 30]. The results showed a successful corroboration with test results indicating that such models can be used as forensic models for assessing the existing conditions as required by various standards and codes.

2 DESCRIPTION OF THE FULL-SCALE REINFORCED CONCRETE JOIST FLOOR

The plan of WSB floor shown in Fig. 1 is for a full-scale reinforced concrete joist floor, designed, constructed and monitored for more than 10 years within the structural laboratories at King Saud University [29, 30]. Fig. 2 is a photo of the floor showing loading and members. The floor consists of wide-shallow beams, one-way joists, a portion of solid slab, and narrow columns that were within the typical widths of masonry walls. Dimensions, main reinforcement, and material properties are given in Table 1.

Testing of the roof slab of the prototype building was done in three stages. Stage 1 was the application of floor self-weight (SW) through form-removal. In Stage 2, a line load of 10.0 kN/m was applied on Joist J19 (WJ19) while in Stage 3, a uniform load (U) of 3.5 kN/m^2 over the entire floor was applied. Concrete blocks were used for load applications. Stages 2 and 3 were applied in a set of mini-intervals where deflections, strains and cracking patterns were collected during and after each interval. Net and accumulated deflections and strains due to immediate load effects were assembled for each stage. The instrumentation plan involves measurement of strains and deflections using various techniques.

The state of cracking on this floor was marked and photographed under all loading stages and throughout their sustained conditions. Examples of the cracked states in the WSB floor were depicted by photos presented in Fig. 3 through Fig. 6. The paths of these cracks were documented by linear measurements of their coordinates to allow plotting them with the numerical results.

Table 1 Floor member dimensions, reinforcement and material properties.

Member	Section dim b x h mm	Longitudinal rebars No of bars x diameter in mm		Ties/stirrups	MPa	MPa
B1, B2	250 x 800	Top	4 φ 16, 11 φ 16 (1)	8@100 mm (4-Leg) at B1 ends	25	511
		Bot	7 φ 16			
B3 , B4	250 x 1200	Top	5 φ 16, 17φ 16(1)	8@100 mm (4-Leg) at B3 ends		
		Bot	9 φ 16			
DB1, DB2	600 x 200	Top	2 φ 16	8@100 mm (2-Leg)		
SS15	h=150	Top	φ 12@550 (2)	None		499
		Bot	φ 16@400(3)			511
J2-J22	250 x 150	Top	1 φ 12	None		499
		Bot	2 φ 14			505
J1& J23 (8)	250 x 200	Top	1 φ 12	None		499
		Bot	2 φ 14			505
C1,C4,C8 (9)	200x 500	8 φ 16		8@200 mm (4-Leg)	28	511
C2	200x 600	8 φ 16		8@200 mm (4-Leg)		511
C3, C6,C7, C9	200x 400	8 φ 14		8@200 mm (4-Leg)		505
C5	200 x 800	10 φ 16		8@200 mm (5-Leg)		511

Notes :(1) rebars at the interior support; (2) in the short direction only; (3) in short and long directions; (4) in the model, J14 was modeled as J1 and J23; (5) orientation as shown in Fig. 1

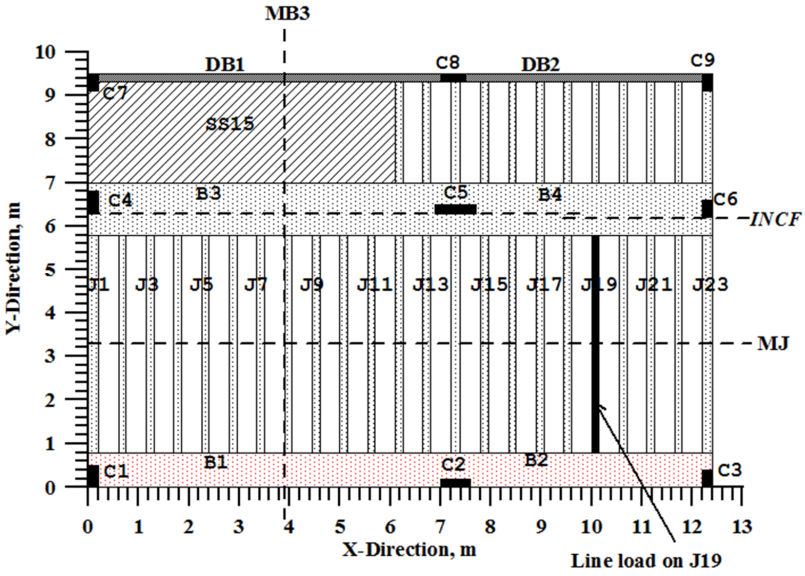

Figure 1 Floor Plan layout, showing member designations

3 SPATIAL AND MATERIAL ASSUMPTIONS OF THE FORENSIC MODEL

Numerical models developed to simulate structure behavior may differ based on the choices made in their spatial modeling, material modeling, element characteristics, and solution procedures. For WSB floor shown in Figures 1 and 2, the nature of the problem is complex and requires three-dimensional for geometrical and material considerations. The complexity may be induced by non-uniformity in floor thickness, existence of columns with eccentricities, different rebar distributions, partial column-floor connections, stirrup arrangements, triaxial effects, and different potential modes of failure. Spatially, concrete can be modeled with a variety of 2-D and 3-D elements. In this study, solid 3-D elements (C3D8) were selected for

Figure 2 A photo of the tested floor showing loading and part of the geometry

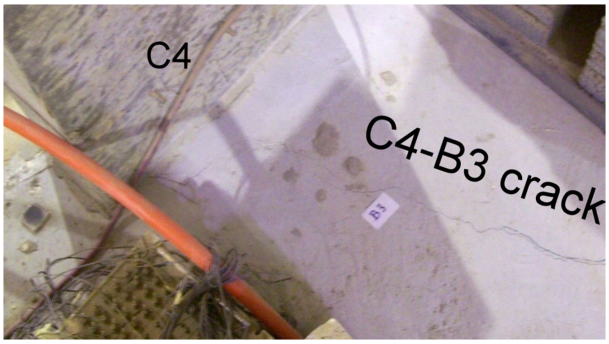

Figure 3 Photographic documentation of crack patterns around C4

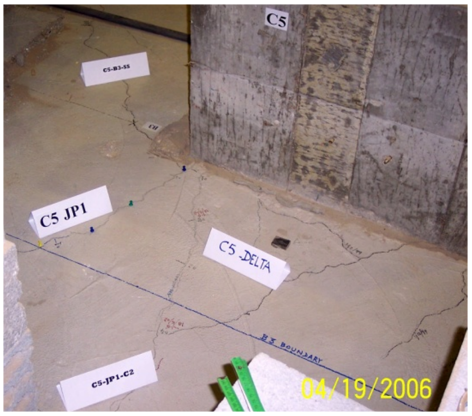

Figure 4 Photographic documentation of crack patterns around C5-long side

concrete while a bi-linear elastic-plastic model was chosen for reinforcing steel and represented in space via truss elements (T3D2). The resulting spatial models for the floor concrete and rebars are presented in Fig. 7 and Fig. 8.

In this study, ABAQUS damage-plasticity model was chosen for modelling concrete behaviour. The post-peak in tension was represented by Hillerborg Fictitious Crack Model (HFCM) (Hillerborg 1985)[21], which is characterized by three key parameters: the specific energy dissipated after the localization in the cracked region; the tensile strength in direct tension; and, the shape assumed for the softening branch. The energy criterion has been employed instead of strength failure criterion in order to minimize the superficial dependence on the chosen finite element.

3.1 Material parameters

The input parameters for the damage-plasticity model of concrete include uniaxial compression curve, uniaxial tensile strength, Poisson's ratio, modulus of elasticity, dilatancy angle, and fracture energy. These parameters were defined as per available test data as well as from appropriate constitutive models from the technical literature [29–32]. The fracture energy,

Figure 5 Photographic documentation of crack patterns on C5-C8 path

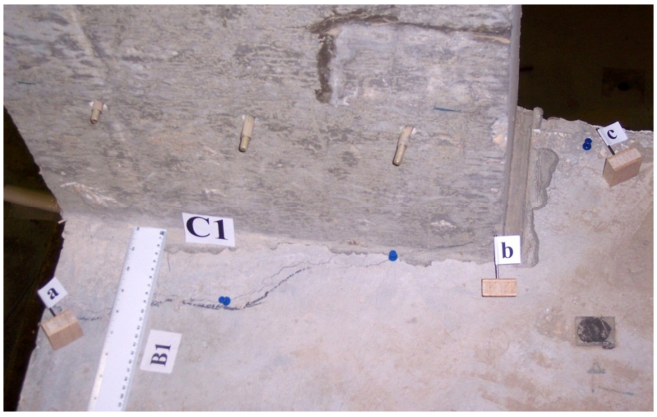

Figure 6 Photographic documentation of crack patterns around C1

G_f, was expressed by Eq. (1) [3]

$$Gf = 110\left(\frac{f_c'}{10}\right)^{0.18} \tag{1}$$

Direct tensile strength, f_t' (MPa) was taken as

$$f_t' = 0.25\sqrt{f_c'} \tag{2}$$

Post-cracking tensile curve for concrete shown in Fig. 9 a was defined by Eq. (3) [25], where n is a coefficient taken as 2.

$$f_t = f_t' = \left(1 - \frac{x}{d_0}\right)^n \; ; \; d_0 = \frac{Gf(n+1)}{f_t'} \tag{3}$$

For uniaxial compression stress-strain curve, the following expression was adopted following

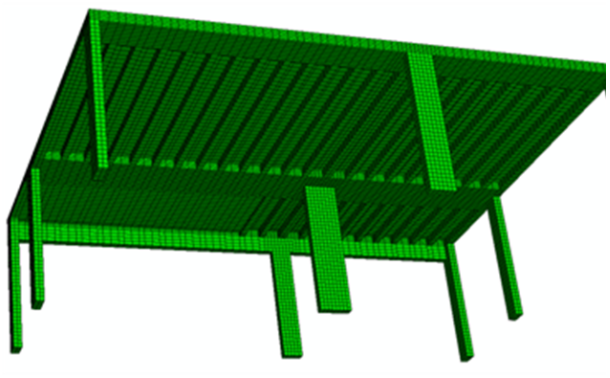

Figure 7 Concrete solid elements and mesh of WSB model.

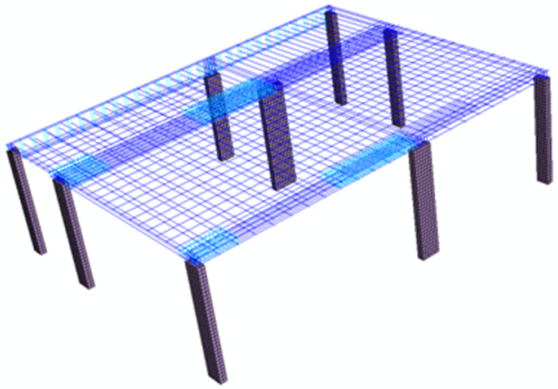

Figure 8 Rebars layout in the WSB model.

Carreira, and Chu (1985)[13]:

$$\frac{fc}{f'_c} = \frac{\beta \frac{\varepsilon}{\varepsilon_0}}{\beta - 1 + \left(\frac{\varepsilon}{\varepsilon_0}\right)^{\beta}};\ where\ \beta = \frac{1}{1 - \frac{f'_c}{\varepsilon_0 E_c}} \tag{4}$$

Where the strain at maximum stress was defined by $\varepsilon_0 = 0.001648 + 0.0000165$, $f_c^{'}$, Ahmed (1981)[10]; and the modulus of elasticity for concrete, E_c(MPa) was given by ACI-363 (1997) [7] $E_c = 3000\sqrt{f'_c} + 6900$. The plastic part of the compression stress-strain curve is shown in Fig. 9 b. The resulting model in its deformed shape along with the contour of maximum principal tensile strains in concrete is shown in Fig. 10.

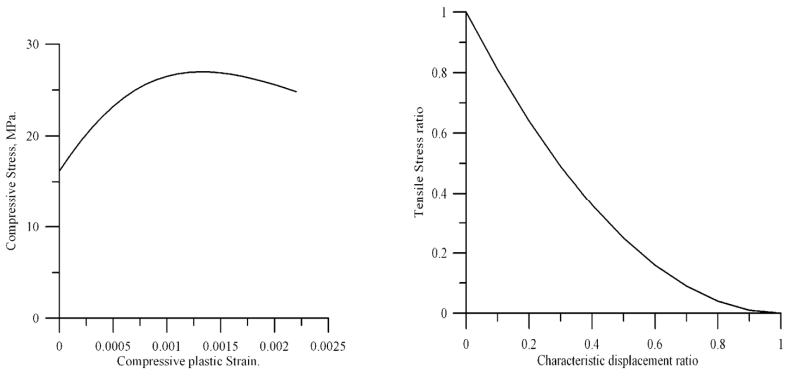

Figure 9 Typical stress-strain curves of concrete; (a) compressive plastic strain vs. stress, (b) post-peak tensile stress vs. displacement

4 FLOOR PHYSICAL CRACKING VERSUS CONCRETE TENSILE STRAINS

Generally speaking, concrete cracking is an elusive phenomenon of complicated nature in the sense of the underlying causes, the significance, and the overall pattern. Cracks may indicate

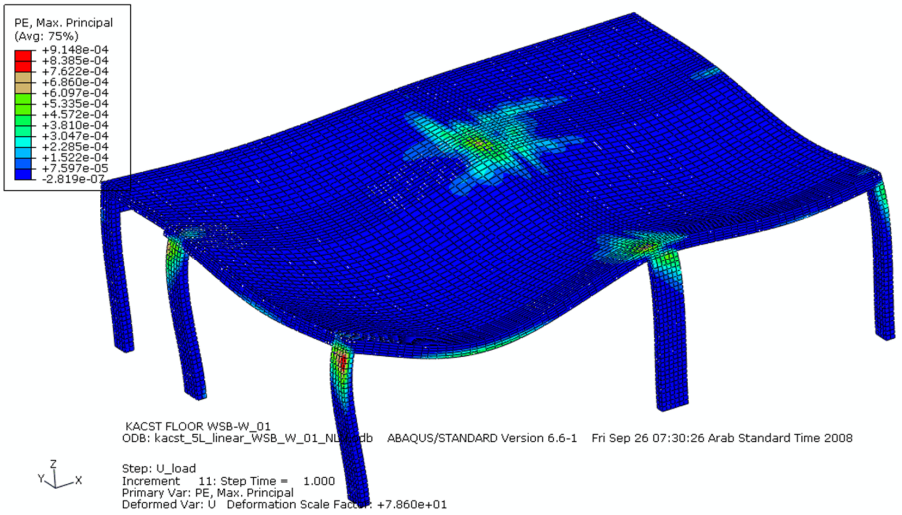

Figure 10 Deformed shape of the floor showing the contour of maximum principal tensile strains in concrete

significant structural distress or a lack of durability. They may also represent the total extent of the damage, or they may point to problems of greater magnitude [6]. In many instances, cracking may be attributed to a combination of stresses due to applied load and restraint of volume change. The path a crack takes is also affected by the concrete composite properties where the aggregate and the interfaces play very important role in the failure process [17].

However, when surveying the damage of an existing structure, the cracking patterns can be detected and documented with reasonable efforts where no particular setup or instrumentations are required. A key quality of a good forensic model is its ability to reproduce existing physical cracks and provide some insight into the underlying causes. The smeared crack approach does not produce actual physical cracks, however, strains or stresses can usually be interpreted, though not directly, to show the potential crack patterns [12, 15, 16, 19, 23, 27, 31–33].

In ABAQUS, cracking is assumed to initiate at points where the tensile equivalent plastic strain is greater than zero, and the maximum principal plastic strain is positive [22]. The direction of the vector normal to the crack plane is assumed to be parallel to the direction of the maximum principal plastic strain. No information can be obtained regarding crack spacing in smeared crack formulation and it may not be a significant issue when investigating large structures at macroscopic level. For the floor of this study, physical major cracks on the top side of the floor were mapped and plotted to a reasonable scale in Fig. 11 through Fig. 14. For direct comparison with the forensic model results, the maximum plastic principal tensile strains (PPTS) were superimposed on the same figures.

4.1 Areas around floor corner columns

The corner columns in this floor had some framing differences affected by the panels they are carrying and the size of beams. Column C1 is part of the largest panel while C3 is in a medium

panel and both are attached to wide shallow beams. On the other hand, C7 is attached to a drop beam carrying solid slab while C9 is part of a joist panels and framing into a drop beam. For the areas around the latter two columns, there is a good correlation between physical observation and model prediction since these areas did not exhibit any physical cracking and no potential of cracking as demonstrated by the lack of noticeable PPTS symbols.

On the other hand, column C1 was surrounded by circumference crack that was reproduced qualitatively through PPTS symbols. This crack was apparently induced by the presence of biaxial negative moment about the x and y-axes. Finally, the crack around C3 was reasonably predicted in a way that is consistent qualitatively with PPTS and in general agreement with the expected crack orientation from the biaxial moment behavior.

4.2 Areas around floor side columns

The floor side columns in this floor include C2, C4, C6, and C8 where the latter is framed into a drop beam while the remaining three were framed into wide shallow beams. Two of these areas are to be discussed next while the other two are to be covered in a subsequent section.

4.2.1 C2 area

Column C2 supports unequal spans (B1 and B2), along its major axis about y-axis. From the floor layout, C2 had the potential also of carrying some moment about its minor x-axis. The area around C2 within the beam width showed several cracks oriented primarily in the y-direction as shown in Fig. 13. From the forensic model, the overall PPTS intensity and orientation were consistent with physical cracks orientations and general location. Following the PPTS symbol convention, the simulated crack should travel in the y-direction in a perpendicular direction to the symbols which were primarily parallel to x-axis.

4.2.2 C8 area

In comparison with C2, the PPTS in the area around C8 showed shorter arrow length, and less intensity indicating that cracking level at C8 should be less than C2. The floor showed a visible crack emerging from the corner of column C8 and another crack crossing the adjacent drop beam (DB1). Having the cracks on the left side of C8 was anticipated because the span of DB1 was larger than the span of DB2. The crack designated C5-C8 extended all over the panel was reproduced by the forensic model as indicated by the PPTS symbols in Fig. 11 and Fig. 12.

4.3 Areas around the interior column

The state of cracking in the area around column C5 was influenced by high intensity of multiaxial moments and shear forces as well as the rectangularity of the column cross-sectional shape. Mapped physical cracks as shown in Fig. 15 revealed that most of the cracks emerged from the vicinities around the column corners. Because of the high aspect ratio of the column section; the short sides became the dominating source of multi-directional cracking. It is to be noted that the overall pattern of the local cracks around C5 resembled to some extent the

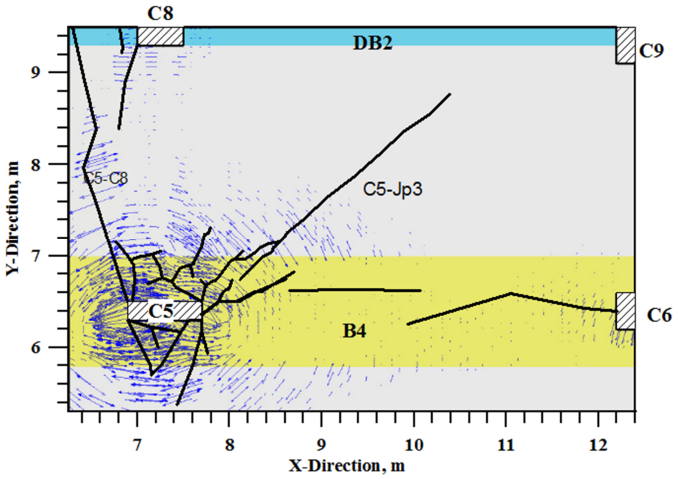

Figure 11 Mapped major cracks along with PPTS in panel C5-C6-C8-C9

state of cracking in a flat plate system on rectangular columns prior to punching shear failure, comprising tangential and diagonal cracks.

Column rectangularity effect on punching shear was recognized by previous studies [8, 24] where the critical shear strength was found to decrease as the aspect ratio increases, such as:

$$v_c = \frac{\left(2 + 3\frac{c_s}{c_l}\right)}{12}\sqrt{f_c'}\ (mpa) \tag{5}$$

where C_s is the short side of the column and C_l is the longer side and $f_c^{'}$ is the concrete strength. The rectangularity effect in this floor was demonstrated by the concentration of cracking around the short sides of the column. This cracking behavior provides a corroboration of previous studies on the effect of column rectangularity on punching shear.

Fig. 15 shows that the overall PPTS intensity and orientation around column C5 is in support of the physical cracks orientations and general location. From this symbolic representation, potential cracks can be viewed to propagate in a perpendicular direction to the two-arrow lines. Fig. 15 shows that the major diagonal cracks to the neighboring panels were clearly predicted except for Jp2 where no physical crack was observed. In general, the forensic model has captured the essence of the behavior to a large extent where the areas covered by PPTS mirrored the areas that were subjected to physical cracks on the actual floor.

5 DESIGN CONSIDERATIONS: CORRELATION OF INTERNAL MOMENTS WITH CRACKING

The complexity of internal moment distribution in concrete slabs has been well recognized; accordingly, codes of practice prescribe certain procedures for approximating the distribution for design purposes. For WSB floors with one-way joist system, the conventional distribution is questionable [29, 30] and it would be appropriate to utilize the forensic model and the

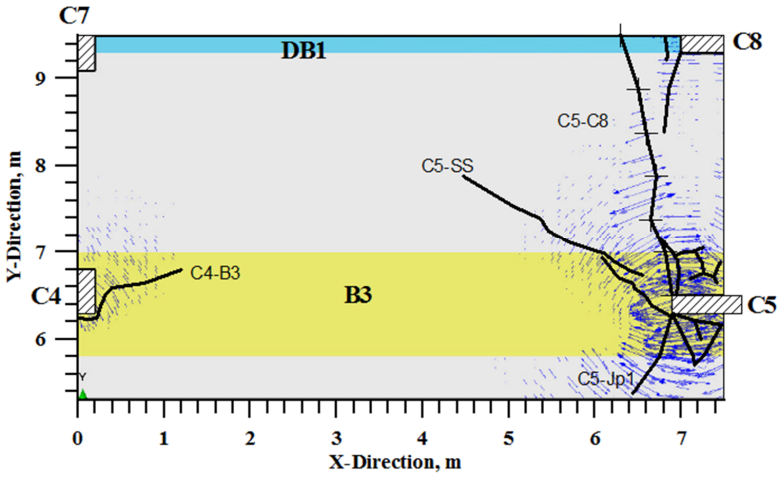

Figure 12 Mapped major cracks along with PPTS in panel C4-C5-C7-C8

experimental findings to verify the internal moment distribution in this floor by correlating with physical cracks and PPTS.

When using solid elements and discrete truss rebar elements, the internal moments and forces are not readily available from the standard output of ABAQUS. Thus, the moments were developed on the basis of the nodal forces and nodal coordinates. A computer post processing program was written for this purpose employing the following fundamental equations with notation as shown in Fig. 16.

Using vector notations,

$$\overrightarrow{M} = \Sigma \overrightarrow{r_n} X \overrightarrow{F_n} = M_x \overrightarrow{\imath} + M_y \overrightarrow{J} + M_z \overrightarrow{k} \tag{6}$$

Where $\overrightarrow{r_n}$ is the position vector from the center of the section to a given node, n.

$$\overrightarrow{r_n} = (\Delta_x)\overrightarrow{\imath} + (\Delta_y)\overrightarrow{j} + (\Delta_z)\overrightarrow{k} \tag{7}$$

where x_0, y_0, and z_0 are the coordinates for the section centroids; x_n, y_n, and z_n are the coordinates for a given node n. similarly, the nodal forces at node n may be written as:

$$\overrightarrow{F_n} = (F_{xn})\overrightarrow{\imath} + (F_{yn})\overrightarrow{j} + (F_{zn})\overrightarrow{k} \tag{8}$$

The moments about x and y axes may be obtained by implementing the cross product of Eq. (6):

$$M_x = \sum_n (y_n - y_0)F_z - (z_n - z_0)F_y$$

$$M_y = \Sigma_n (z_n - z_0)F_x - (x_n - x_0)F_z \tag{9}$$

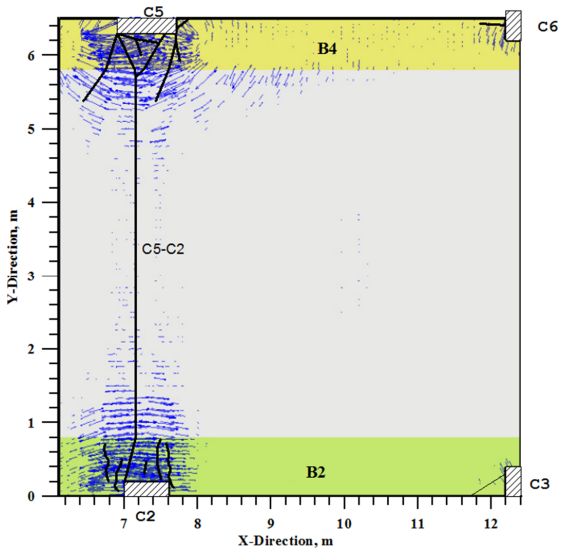

Figure 13 Mapped major cracks along with PPTS in panel C2-C3-C5-C6

The moment diagrams about y-axis and x-axis over the interior shallow wide member beam B3-B4 are shown in Fig. 17 and it is of interest to examine the correlation of these moments with physical cracks. Under the sign convention used in this study, negative moment exceeding the cracking moment about x-axis (M_x) should produce top cracking along x-axis (i.e along the beam) while negative moment about y-axis (M_x) should produce cracking along y-axis (i.e across the beam). Their relative values can influence the direction and path of the crack on the beam.

First, Fig. 17 reveals that the exterior end of B3 is subjected to a higher intensity of (M_x) moment coupled with a low intensity of (M_y); this distribution favors cracks in the x-direction which was consistent with the observed crack (C4-B3) in Fig. 12. Second, the middle part of B3 has positive moment and negligible negative moment (M_x) suggesting that no cracks should be expected on the top side of B3. As expected, the floor did not exhibit cracks on the middle portion of B3 corroborating the results from the forensic model.

Third, for the middle and exterior portion of B4, the figure shows that the moment (M_x) is negative with appreciable value in comparison to its counterpart on B3; moreover, the moment (M_y) is either positive or of negligible negative value. This situation calls for cracking along B4, and this was the observed pattern. Finally, Fig. 17 shows that the interior ends of B3 and B4 were subjected to high negative moments about both axes inducing multi-directional cracking, as observed.

Thus, in addition to diagnosis of the existing floor conditions, the information revealed about the internal distribution of moments indicated that the common simplified procedure for one-way joist floor system which assumes a uniform intensity of (M_x) was unrealistic and contradicted by the forgoing profile. This discrepancy between the assumption and the actual distribution was investigated by [30] and a new design procedure has been proposed.

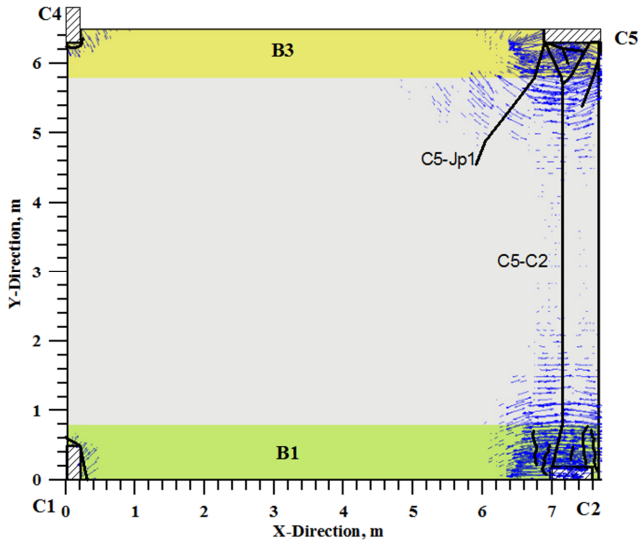

Figure 14 Mapped major cracks along with PPTS in panel C1-C2-C4-C5

6 FLOOR DEFLECTIONS: VERIFICATION AND INTERPRETATIONS

For further corroboration of the analytical forensic model with test results, vertical deflection profiles along two lines in the floor were examined. Deflections are among the key behavioral aspects and the ability of a forensic model to produce a reliable assessment of such large scale test is of a great value in terms of validation and behavior interpretation. The deflections profiles along line MJ and line MB3 are plotted in Fig. 18 and Fig. 19, respectively. It can be observed that the forensic model produced deflections that were in good agreement with test results for the three loading stages. The three experimental measuring schemes (dial gauges (DG), LVDT, and surveying technique (SVY)) employed in this study produced very consistent results with some expected scatter in readings. The agreement in trend and magnitude between experimental and the forensic model had implication on mutual validation of test measurements and numerical predictions.

Moreover, deflection results can be interpreted to shed some light on the long crack from C2 to C5 and that from C5 to C8, recognizing the role of edge members rigidities on the slab panel behavior. For a typical rectangular slab panel, the load transfer and distribution of moments in the two-directions is governed by the rigidity of edge members and panel continuity. This principle remains true to some extent for rectangular joist panel; although, joist panels have more complexity due to the interaction between unidirectional ribs and the top slab panel that represents the flange.

For the panel bounded by columns C1, C2, C4, and C5, the portion of the joist panel connecting column C2 to C5 represents a de facto supporting member due to its high rigidity as influenced of the two columns. This high rigidity can be interpreted from the deflection profile along MJ line (Fig. 18) where the panel edges are marked by lower relative deflection in comparison to mid-panel. It follows that a negative moment will form about y-axis on line

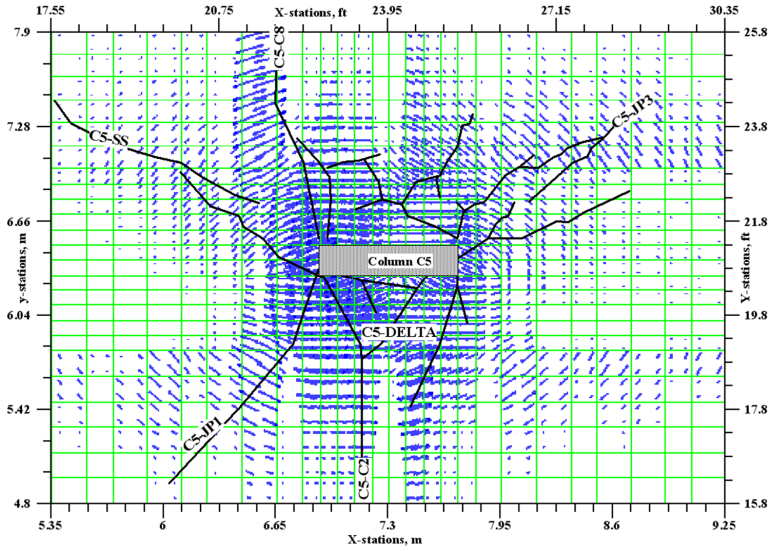

Figure 15 Mapped major cracks around column C5 along with PPTS

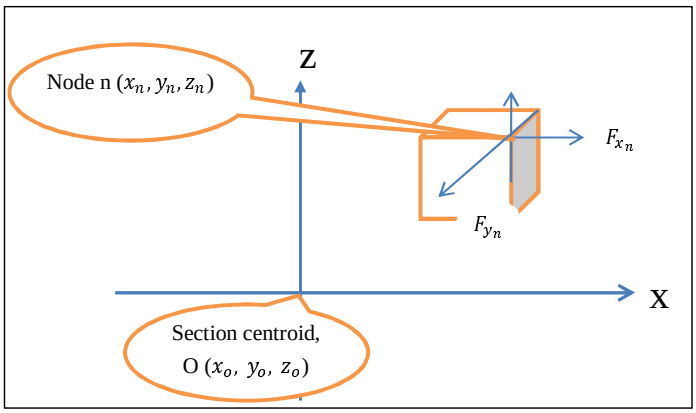

Figure 16 Computation of section moments from solid nodal forces

C2-C5, and since the flange is weak in resisting the moment, cracking has to take place. The panel behavior may also be viewed in terms of compatibility requirements where the joist panel needs to deform in a compatible way with the beams B1 and B3.

From the forgoing discussion, deflections were properly produced by the forensic model and the results were shown to correlate with cracking along line C2-C5-C8. Even though some concerns have been raised about NLFE, forensic models in the framework of plasticity-damage approach and Hillerborg Fictitious Crack Model (HFCM) as supplemented by appropriate constitutive expressions provided a powerful, accurate platform that can be used for forensic assessment of distressed or failed reinforced concrete structures.

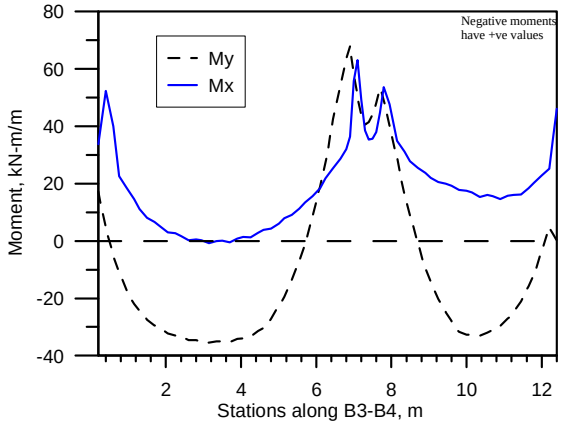

Figure 17 Moment profiles about x and y-axes along beams B3 and B4

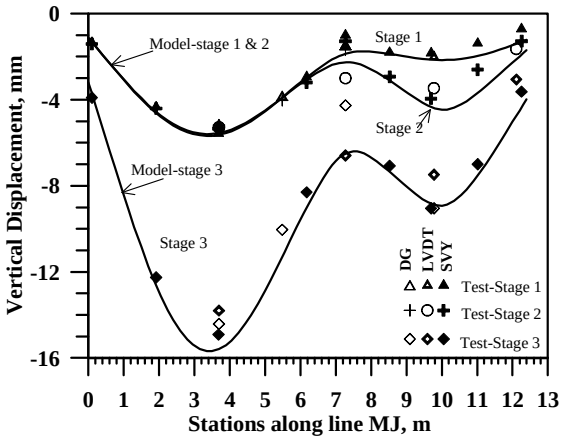

Figure 18 Deflection profile along line MJ in WSB model and tested floor

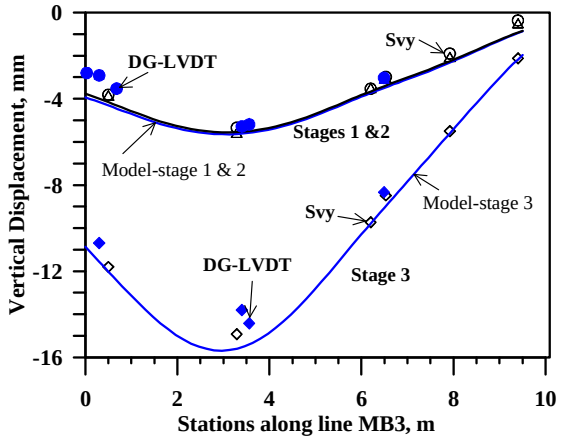

Figure 19 Deflection profile along line MB3 in WSB model and tested floor

7 SUMMARY AND CONCLUSIONS

This paper presented the results of an investigation on the diagnosis and assessment of an existing structure employing a nonlinear forensic model. Various standards consider numerical diagnosis as a major stage in the assessment and strengthening of existing structures based on which several decisions involving safety and economical aspects are made. Accordingly, an integral part of the methodology is to verify the forensic model reliability through comparison with realistic large-scale tests. This was done in this study by investigating one-story floor of joist-construction style with hidden wide shallow beams supported on elongated columns. Based on this investigation, the following points can be made:

1. The forensic model and the experiment agreed on the behavior at macroscopic level in terms of deflections and cracking patterns. Concrete principal plastic tensile strain (PPTS) was shown to be a good indirect indicator of cracking patterns in terms of cracking location and direction through symbolic representation. However, identifying the underlying reasons of major cracks in the floor required correlating with other key field parameters including deflections, and internal moments.

2. The ability of the forensic model to reproduce the surveyed damage state of the floor provided a positive indication on the material models, spatial representation, and parameter selection. Spatially, well-balanced mesh of concrete and rebar elements was shown to be sufficient to provide reasonably accurate information. Having extremely fine mesh as usually performed on individual members is not practical neither seemed necessary for 3-D buildings. The plasticity-damage approach combined with HFCM and supplemented by appropriate constitutive expressions provided robust model.

3. The distribution of internal moments about the longitudinal axis of the wide shallow beams (M_x) was of variable nature and consistent with the observed cracking patterns. This finding confirmed the need to improve the design methodology of one-way joist systems on wide shallow beams, as proposed elsewhere [30].

Acknowledgments The author gratefully acknowledges the support provided by King AbdulAziz City for Science & Technology under Grant No. AR-16-66 in the experimental work. Any opinions, findings, and conclusions expressed in this paper are those of the writers and do not necessarily reflect the views of the sponsor.

References

[1] FIB Bulletin 14. Externally bonded frp reinforcement for rc structures. Technical report, FIB, Lausanne, Switzerland, 2001.

[2] ACI-440 2R. *Design and construction of externally bonded FRP systems for strengthening concrete structures.* Farmington Hills, MI, 2008.

[3] Fib Bulletin 42. Constitutive modelling of high strength / high performance concrete. state-of-art report by task group 8.2. Technical report, International Federation for Structural Concrete, Lausanne, Switzerland, 2008.

[4] ASCE-ACI Committee 447. State of the art report on finite element analysis of reinforced concrete, 1982.

[5] ASCE-ACI Committee 447. Finite element analysis of reinforced concrete structures ii, 1993.

[6] ACI-224.1R. *Causes, evaluation, and repair of cracks in concrete structures*. Farmington Hills, MI, 26 edition, 2007.

[7] ACI-363R-92. *State of the art report on high strength concrete*. Farmington Hills, MI, 55 edition, 1997.

[8] ACI-426. *"The shear strength of reinforced concrete members" Part 4 of ACI manual of concrete practice*. Farmington Hills, MI, 1987.

[9] ACI-446. *Finite Element Analysis of Fracture in Concrete Structures: State-of-the-Art*. Farmington Hills, MI, 1997.

[10] S. H. Ahmed. *Properties of confined concrete subjected to static and dynamic loading*. PhD thesis, University of Illinois at Chicago, 1981.

[11] F. Bencardino, L. Rizzuti, and G. Spadea. Strengthening/retrofitting of an rc structure with bonded cfrp laminates: reliability evaluation using different guidelines. *FRPRCS-8*, July 16-18 2007.

[12] P. Bhatt and M. Abdel Kader. Prediction of shear strength of reinforced concrete beams by nonlinear fnite element analysis. computers and structures. *Computers and Structures*, 68:139–155, 1998.

[13] D. J. Carreira and K. Chu. Stress-strain relationship for plain concrete in compression. *ACI Journal*, 82:797–804, 1985.

[14] W. F. Chen and D. J. Han. *Plasticity for Structural Engineers*. Springer-Verlag, New York, 1988.

[15] D. Coronelli and M. G. Mulas. Modeling of shear behavior in reinforced concrete beams. *ACI Structural Journal*, 103(3):372–382, 2006.

[16] R. de Borst. Fracture in quasi-brittle materials: a review of continuum damage-based approaches. *Engineering Fracture Mechanics*, 69:95–112, 2002.

[17] G. Giaccio and R. Zerbino. Failure mechanism of concrete: combined effects of coarse aggregates and atrength level. *Advanced Cement Based Materials*, 7(2):41–48, 1998.

[18] P. Grassl and M. Jirasek. Damage-plastic model for concrete failure. *International Journal of Solids and Structures*, 43:7166–7196, 2006.

[19] A. D. Hanganu, E. Onate, and A. H. Barbat. A finite element methodology for local/global damage evaluation in civil engineering structures. *Computers and Structures*, 80:1667–1687, 2002.

[20] Hibbitt, Karlsson & Sorensen, Inc., Pawtucket, RI. *ABAQUS Users' Manuals and Theory Manual Version 6.10*, 42 edition, 2009.

[21] A. Hillerborg. The theoretical basis of a method to determine the fracture energy gf of concrete. *Materials and Structures*, 18:291–296, 1985.

[22] J. Lubliner, J. Oliver, and S. Oller. A plastic-damage model for concrete. *International Journal of Solids and Structures*, 25(3):229–326, 1989.

[23] P. Menetrey. Synthesis of punching failure in reinforced concrete. *Cement & Concrete Composites*, 24:497–507, 2002.

[24] J. Moe. *Shearing Strength of Reinforced Concrete Slabs and Footings under Concentrated Loads*. Development Department Bulletin D47, Portland Cement Association, 1961.

[25] R. C. Murthy, G. S. palani, and R. Riyer. State-of-the-art review on fracture analysis of concrete structural components. *Sadhana*, 34(2):345–367, 2009.

[26] G. D. Nguyen and A. M. Korsunsky. Development of an approach to constitutive modelling of concrete:isotropic damage coupled with plasticity. *International Journal of Solids and Structures*, 45:5483–5501, 2008.

[27] J. Pamin and R. de Bort. Simulation of crack spacing using a reinforced concrete model with an internal length paamter. *Archive of Applied Mechanics*, 68:613–625, 1998.

[28] T. Sain and J.M. Chandra Kishen. Energy-based equivalence between damage and fracture in concrete under fatigue. *Engineering Fracture Mechanics*, 74:2320–2333, 2007.

[29] A. B. Shuraim and A. I. AL-Negheimish. Influence of wide-shallow-beam flexibility on joist-floor behavior. In *Proceedings of the Third International Conference on Modeling, Simulation and Applied Optimization*, Sharjah, U.A.E, January 20-22 2009. paper 89099.

[30] A. B. Shuraim and A. I. AL-Negheimish. Design considerations for joist-floors with wide-shallow-beams. *ACI Structural Journal*, 108(2):188–196, 2011.

[31] Ahmed Shuraim. Three-dimensional non-linear modelling aspects of a full-scale reinforced concrete banded-joist floor. In *Proceedings of the Eighth International Conference on Computational Structures Technology*, 2006. paper 13.

[32] Ahmed B. Shuraim. Efficacy of CFRP configurations for shear of RC beams. *Structural Engineering and Mechanics*, 39(3):361–382, 2011.

[33] F. J. Vecchio. Analysis of shear-critical reinforced concrete beams. *ACI Structural Journal*, 97(1):102–110, 2000.

[34] F. J. Vecchio. Non-linear finite element analysis of reinforced concrete: At the crossroads? *Structural Concrete*, 2(4):201–212, 2001.

[35] F. J. Vecchio, E. C. Bentz, and M. P. Collins. Tools for forensic analysis of concrete structures. *Computers and Concrete*, 1(1):1–14, 2004.